

Fast Blast Wave and Ejecta in the Young Core-Collapse Supernova Remnant MSH 15-52/RCW 89

KAZIMIERZ J. BORKOWSKI,¹ STEPHEN P. REYNOLDS,¹ AND WILLIAM MILTICH¹

¹*Department of Physics, North Carolina State University, Raleigh, NC 27695-8202, USA*

(Received 2020 April 10; Revised 2020 May 6; Accepted 2020 May 11)

ABSTRACT

One of the youngest known remnants of a core-collapse supernova (SN) in our Galaxy is G320.4–1.2/MSH 15-52, containing an energetic pulsar with a very short (1700 yr) spindown age and likely produced by a stripped-envelope SN Ibc. Bright X-ray and radio emission north of the pulsar overlaps with an H α nebula RCW 89. The bright X-rays there have a highly unusual and quite puzzling morphology, consisting of both very compact thermally emitting knots and much more diffuse emission of nonthermal origin. We report new X-ray observations of RCW 89 in 2017 and 2018 with *Chandra* that allowed us to measure the motions of many knots and filaments on decade-long time baselines. We identify a fast blast wave with a velocity of $(4000 \pm 500)d_{5.2}$ km s⁻¹ ($d_{5.2}$ is the distance in units of 5.2 kpc) with a purely nonthermal spectrum, and without any radio counterpart. Many compact X-ray emission knots are moving very fast, with velocities as high as 5000 km s⁻¹, predominantly radially away from the pulsar. Their spectra show that they are Ne- and Mg-rich heavy-element SN ejecta. They have been significantly decelerated upon their recent impact with the dense ambient medium north of the pulsar. We see fast evolution in brightness and morphology of knots in just a few years. Ejecta knots in RCW 89 resemble those seen in Cas A at optical wavelengths in terms of their initial velocities and densities. They might have the same origin, still not understood but presumably related to stripped-envelope SN explosions themselves.

Keywords: Supernova remnants (1667); Core-collapse supernovae (304); Ejecta (453); Rotation powered pulsars (1408); X-ray astronomy (1810);

1. INTRODUCTION

A significant fraction of massive stars shed part or all of their hydrogen envelope before explosion ($\sim 30\%$ of core-collapse supernovae (SNe) are of Type IIb, Ib, or Ic; e.g. Shivvers et al. 2017). The mechanisms of mass loss are not well understood. The supernova remnant (SNR) Cassiopeia A is now generally thought to have resulted from a SN Ib, based on light-echo observations (Krause et al. 2008; Rest et al. 2011). Cas A exhibits the presupernova wind as quasi-stationary “focculi” rich in N, but also high-velocity knots of O-rich ejecta. The dense ejecta knots may hold clues to instabilities in the explosion itself. Older objects that probably resulted from stripped-envelope events include the complex remnant MSH 15–52/RCW 89, the subject of this Letter.

Our target was discovered as a large ($\sim 32'$ diameter) radio source (MSH 15–52; Mills et al. 1961), consisting of a fairly bright northern region and fainter southern region (Caswell et al. 1981), the northern one coincident with a filamentary H α nebula, RCW 89 (Rodgers et al. 1960). The source contains one of the most extreme rotation-powered pulsars, with a surface field of 1.5×10^{13} G and the third-shortest known spindown timescale (about 1700 yr): PSR B1509-58 (see data in Kargaltsev et al. 2013), which possesses a peculiar, anisotropic pulsar-wind nebula (PWN) in X-rays, though radio observations (Gaensler et al. 1999) showed no clear coun-

terpart. For a distance of 5.2 kpc (Gaensler et al. 2002), the distance from the pulsar to the northern optical extent of RCW 89 is about 23 pc. At that distance, the required expansion velocity is about 13,000 km s⁻¹, though optical knots have negligible expansion speeds (van den Bergh & Kamper 1984).

Chandra observations (Gaensler et al. 2002) have shown that RCW 89 was bright in X-rays, with many small bright knots of emission not well correlated with optical knots, but in some cases coincident with radio knots (Gaensler et al. 1999). Gaensler et al. (1999) argued convincingly that the MSH 15–52/RCW 89 complex is in fact a single SNR, and that its large size and young age could be understood as the result of a stripped-envelope supernova (SN Ibc), a suggestion seconded by Chevalier (2005). A Sedov blast wave could reach the required radius in 1700 yr for an upstream density of ~ 0.04 cm⁻³, perhaps understandable as the stellar-wind bubble blown by the progenitor. In that case, the total swept-up mass is $\sim 9M_{\odot}$ and the current shock velocity is $0.4R/t \sim 3000$ km s⁻¹.

Yatsu et al. (2005) showed that the X-ray knots have individual, differing thermal spectra, based on the original 2000 20 ks *Chandra* observation. In an unpublished PhD thesis, Yatsu (2008) attempted to measure proper motions (PMs) between two *Chandra* images from 2000 and 2004, with some

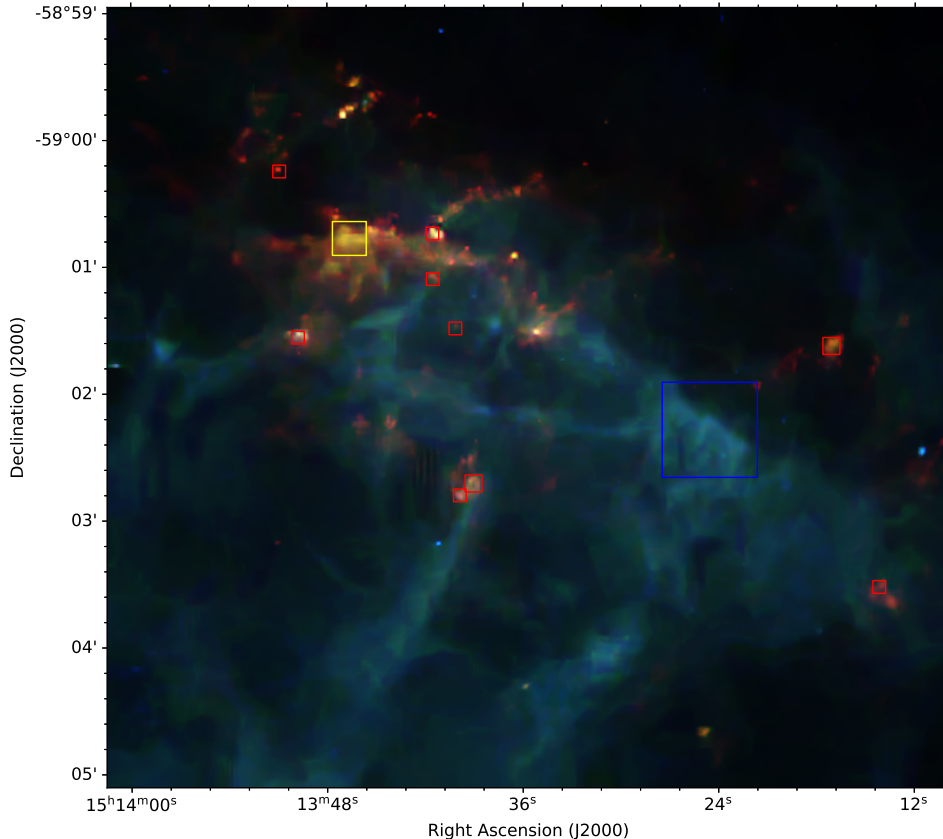


Figure 1. *Chandra* image of RCW 89 in 2018 (red: 0.5–2 keV; green: 2–3 keV; blue: 3–6.5 keV). Soft, thermally emitting compact ejecta knots are in sharp contrast to diffuse and hard X-rays of nonthermal origin. Boxes enclose knots and filaments selected for PM measurements (see their blowups in Figure 2).

success, finding velocities of some knots of order 4000 km s^{-1} , in contrast with the low velocities of optical knots, but consistent with the young age of RCW 89. However, the far off-axis position of RCW 89 for one of the observations resulted in large uncertainties.

These contradictory findings raise various important questions. Where is the blast wave? What are its properties? Can we find and identify SN ejecta, and distinguish them from shocked ambient medium? What is the nature of the interaction of the PWN with ejecta? Is further particle acceleration to TeV energies occurring, as is observed in all SNRs as young as RCW 89? To explore these questions, we obtained a 185 ks observation of RCW 89 in 2017 and 2018, as described below.

2. OBSERVATIONS

RCW 89 was observed by *Chandra* in 2004 December for 29 ks, and 2008 June for 59 ks. Deep (184 ks effective exposure time) third-epoch observations of RCW 89 include four individual pointings between 2017 December 27 and 2018 February 13 and a final fifth pointing in 2018 April 8–9 (for brevity, we hereafter refer to these five pointings as the 2018 observations). In all observations, RCW 89 was placed on the Advanced CCD Imaging Spectrometer (ACIS) S3 chip, with

Very Faint mode used to reduce the particle background. No significant particle flares were found.

We aligned individual third-epoch pointings using bright and compact emission knots (see Figure 1). The inter-epoch alignment was done by matching positions of several point sources near the *Chandra* optical axis. We jointly fit them with 2D Gaussians to arrive at best estimates of image shifts between the epochs, with statistical 1σ errors in alignment not exceeding 0.1 ACIS pixels in R.A. and decl. (ACIS pixel size is $0''.492 \times 0''.492$). These errors translate into PM errors in R.A. and decl. below 5 mas yr^{-1} , given the (exposure-weighted) time baselines of 13.09 (9.62) yr between the 2004 (2008) and 2018 observations.

After alignment, we extracted images and spectra from event files. The individual 2018 event files were merged together prior to image extraction, but spectra were extracted separately from each individual event file. We then summed them together and averaged their spectral and ancillary responses by weighting them by individual exposure times.

3. EXPANSION

Motions of most compact emission knots can be readily discerned by eye: see Figure 2 for a number of selected knots, and Figures 1 and 3 for their location within RCW 89. Additionally, morphologies of many knots have changed over time

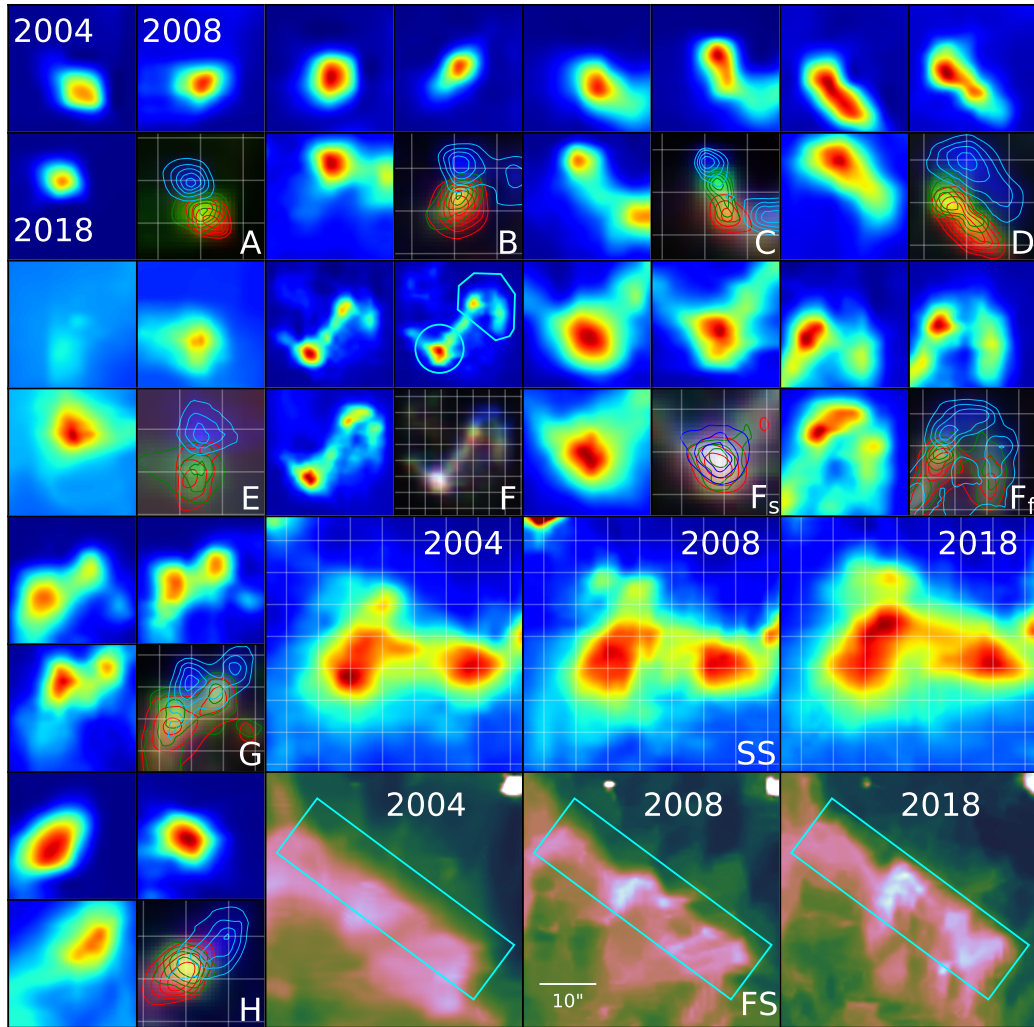


Figure 2. Selected emission knots and filaments in 2004, 2008, and 2018. Their large motions are apparent. RGB images (bottom right of each knot’s panels, except for regions SS and FS), with contours and coordinate grids drawn over, show them in more detail (red–2004, green–2008, blue–2018). Knots F_s (bottom left) and F_f (top right) are within regions drawn over the 2008 image in panel F. Region FS (in cyan) is where we measured motion of the fast X-ray synchrotron emitting blast wave. Each coordinate grid cell is $2'' \times 2''$ in size.

(knot F_f is an extreme example). Several knots have either brightened, including knot A, or faded (e.g., knots B and H), by up to a factor of several for both fading and brightening knots. Entirely new ejecta knots appeared in 2018, including new knots adjacent to knot B and a bright knot northwest of knot C at R.A. = $15^{\text{h}}13^{\text{m}}41^{\text{s}}.1$ and $\delta = -59^{\circ}00'38''$.

PMs were first independently measured on each of the two (13.1 and 9.6 yr) long time baselines, and then combined (except for region FS; see below). After extracting broadband (0.5–6.5 keV) images, $359'' \times 359''$ in size and with $0''.175 \times 0''.175$ image pixel, we used the iterative variance-stabilization method of Azzari & Foi (2016) to smooth them (parts of these smoothed images are shown in Figure 2). Except for knots E and H, we then used a smoothed image from one epoch and an unsmoothed image from another epoch to measure motions, modeled as simple image shifts but also allowing for brightening or fading through an overall change

in the mean surface brightness between the epochs. Poisson statistics were assumed for unsmoothed images. A maximum likelihood method was employed, with smoothed images used as models, and with unsmoothed data taken only from small regions encompassing measured knots. On each of the time baselines, we computed a signal-to-noise ratio-weighted PM from measurements based on two smoothed and unsmoothed image pairs, with unsmoothed data and smoothed models alternately taken from each of the two epochs. Errors were added in quadrature, so the counting noise at each epoch was taken into account. But for faint and compact knots, smoothing of images results in a significant loss in precision. Knot E is the faintest and most compact among the knots shown in Figure 2, while knot H has faded considerably since 2004 and 2008. So for these two knots, we just fit a 2D Gaussian (+ constant background) to unsmoothed data at each epoch (again using C-statistics; Cash 1979), then

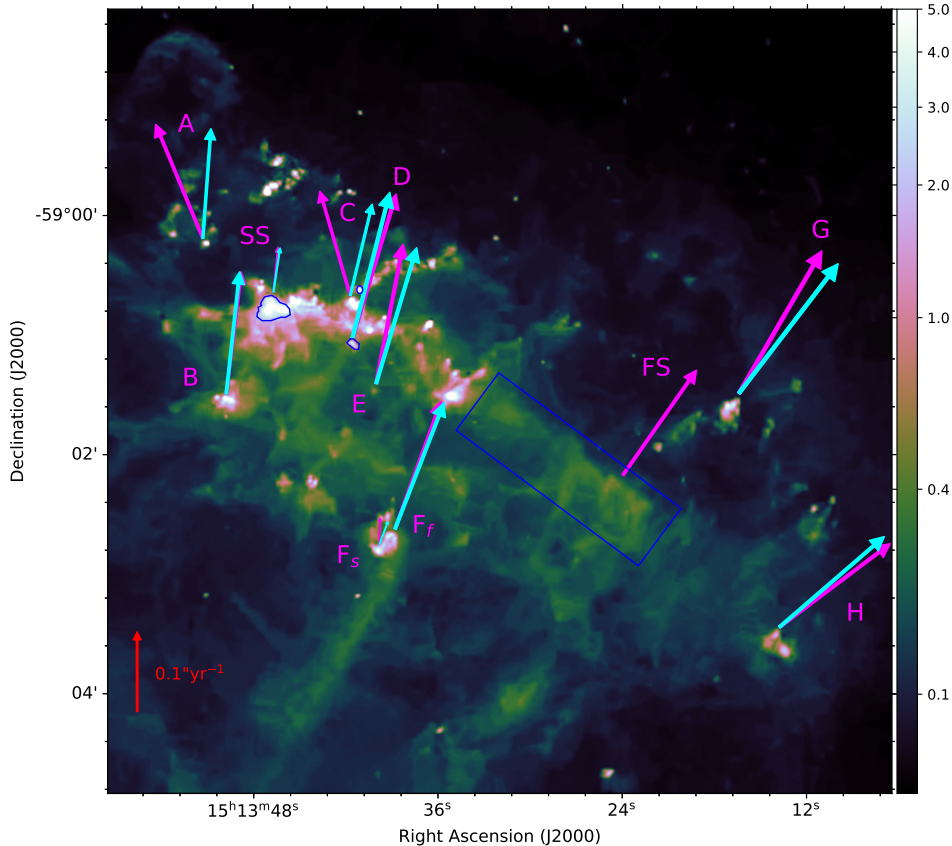


Figure 3. PMs (magenta arrows, not to scale), and their radial components with respect to the pulsar (cyan arrows), drawn over the broadband (0.5–6.5 keV) *Chandra* image. The scaling is shown by red arrow pointing radially away from the pulsar. The four regions (in blue) are where we extracted spectra shown in Figure 4. The scale is in counts per $0''.192 \times 0''.192$ image pixel.

calculated shifts of Gaussian peaks between the epochs and converted them into PMs.

Results of our PM measurements can be found in columns (2) and (4) in Table 1. Only statistical errors are listed; neither errors in alignment or (unknown but likely substantial) systematic errors are taken into account. The final results in columns (3) and (5) are obtained by combining PMs (after adding in quadratures the 5 mas yr^{-1} alignment error in each individual measurement). We also list in Table 1 radial and tangential PM components with respect to the pulsar, μ_r and μ_t , angular distances of knots from the pulsar, (radial) expansion rates, deceleration parameters m (products of expansion rates and the estimated remnant’s age), and radial and tangential velocities v_r and v_t .

Motion of a low surface brightness filament within region FS can also be discerned by eye (Figure 2), but its measurement requires use of a different, more advanced technique. Presumably, this filament is a fast blast wave moving radially away from the pulsar. In order to measure its radial motion, we used a Bayesian method that we had employed previously in our study of the very young remnant G330.2+1.0 (Borkowski et al. 2018). Briefly, we used the smoothed 2018 image (shown at the right-hand corner of Figure 2) as a model that was allowed to expand or shrink,

and also vary in its mean surface brightness, with the expansion centered on the pulsar. Unsmoothed 2004 and 2008 data were jointly fit by this model, assuming a constant expansion rate across all epochs. In order to verify this assumption, we also measured expansion rates based only on two-epoch baselines. The mean expansion rate is $0.0329^{+0.0047}_{-0.0048} \% \text{ yr}^{-1}$ for the 2008–2018 baseline, and $0.0494^{+0.0057}_{-0.0059} \% \text{ yr}^{-1}$ for the 2004–2018 baseline (errors are 68% credible intervals). These rates are in reasonable agreement with the rate of $0.0374^{+0.0044}_{-0.0044} \% \text{ yr}^{-1}$ (see column (9) of Table 1) based on the joint fit using data from all three epochs.

Our measured PMs are shown Figure 3, with their radial components with respect to the pulsar. The fastest ($\mu_r = 205 \pm 6 \text{ mas yr}^{-1}$, $v_r = 5060 \pm 120 d_{5.2} \text{ km s}^{-1}$) knot G is also the most distant of our knots from the pulsar. Its motion is nearly radial, but there is a statistically significant ($v_t = -650 \pm 140 d_{5.2} \text{ km s}^{-1}$) tangential component. Its deceleration parameter m of 0.71 is much less than unity. Its complex morphology has changed somewhat since 2004, suggesting the presence of significant internal motions and/or brightness variations. Other very fast-moving ($v_r > 4000 d_{5.2} \text{ km s}^{-1}$) knots D, E, F_f , and H are moving radially away from the pulsar, but with m still less than 1. Knot F_f that is located closer to the pulsar might be some-

Table 1. PMs and Expansion Rates

Region	$\mu_\alpha \cos \delta^a$ ("yr ⁻¹)		μ_δ^a ("yr ⁻¹)		μ_r^b ("yr ⁻¹)	μ_t^c ("yr ⁻¹)	Distance (")	Expansion Rate (% yr ⁻¹)	m^d	v_r^e (km s ⁻¹)	v_t^e (km s ⁻¹)
(1)	(2)	(3)	(4)	(5)	(6)	(7)	(8)	(9)	(10)	(11)	(12)
A	0.059(4) 0.058(8)	0.059(5)	0.136(4) 0.156(7)	0.143(5)	0.139(5)	-0.070(5)	476	0.0291 ± 0.0011	0.50	3420 ± 120	-1720 ± 130
B	-0.017(3) -0.022(4)	-0.019(4)	0.149(3) 0.157(4)	0.153(4)	0.154(4)	0.002(4)	400	0.0384 ± 0.0011	0.66	3790 ± 110	60 ± 110
C	0.041(4) 0.037(3)	0.038(4)	0.152(3) 0.111(3)	0.131(4)	0.118(4)	-0.068(4)	459	0.0258 ± 0.0009	0.44	2920 ± 100	-1670 ± 110
D	-0.047(6) -0.068(9)	-0.055(6)	0.182(6) 0.179(8)	0.181(6)	0.189(5)	0.008(7)	439	0.0431 ± 0.0012	0.74	4660 ± 130	200 ± 160
E	-0.034(22) -0.030(20)	-0.034(17)	0.137(28) 0.195(20)	0.175(15)	0.178(17)	-0.018(16)	418	0.0425 ± 0.0040	0.73	4380 ± 380	-440 ± 420
F _s	-0.004(6) 0.004(8)	-0.001(6)	0.034(7) 0.031(7)	0.033(6)	0.031(6)	-0.011(6)	343	0.0090 ± 0.0016	0.15	760 ± 140	-270 ± 150
F _f	-0.062(7) -0.051(8)	-0.058(6)	0.172(8) 0.149(8)	0.160(7)	0.170(7)	-0.005(6)	351	0.0485 ± 0.0020	0.83	4190 ± 170	-130 ± 140
G	-0.102(5) -0.106(6)	-0.104(6)	0.180(6) 0.178(6)	0.179(5)	0.205(6)	-0.026(5)	494	0.0415 ± 0.0011	0.71	5060 ± 120	-650 ± 140
H	-0.136(9) -0.145(12)	-0.139(8)	0.105(9) 0.105(12)	0.105(8)	0.174(9)	0.011(7)	424	0.0410 ± 0.0022	0.70	4290 ± 230	280 ± 170
SS	-0.010(6) -0.001(8)	-0.006(6)	0.054(5) 0.057(5)	0.056(5)	0.056(5)	-0.002(6)	448	0.0124 ± 0.0011	0.21	1380 ± 120	-60 ± 150
FS	0.161(19)	...	430	0.0374 ± 0.0044	0.64	3970 ± 460	...

NOTE—Errors are 1σ . PM errors (in mas yr⁻¹) are listed in parentheses.

^aLeft column: PMs based on the 2004–2018 (top) and 2008–2018 (bottom) time baselines. Right column: combined PM.

^bRadial PM.

^cTangential PM, positive (negative) for clockwise (counter-clockwise) motion.

^dDeceleration parameter (assuming remnant’s age is equal to the pulsar’s characteristic age of 1710 yr; Livingstone & Kaspi 2011).

^eVelocity is $v_{5.2}d_{5.2}$, with $d_{5.2}$ the distance in units of 5.2 kpc.

what less ($m = 0.83$) decelerated. Another radially moving and rapidly varying knot, knot B, appears to be somewhat slower ($\mu_r = 154 \pm 4$ mas yr⁻¹, $v_r = 3790 \pm 110d_{5.2}$ km s⁻¹) and more ($m = 0.66$) decelerated than other radially moving fast knots. Finally, still slower and more decelerated knots A and C exhibit strongly nonradial motions. We caution here that for rapidly brightening (or fading) knots such as knot A our measured motions might not necessarily reflect the bulk ejecta motions. Nevertheless, nonradial motions, brightening and fading, and changes in knot morphologies are all consistent with the fast-moving, dense ejecta clumps being rapidly decelerated after a sudden encounter with a dense ambient medium north of the pulsar.

The closest knot to the pulsar whose motion we measured, knot F_s, stands apart from other compact knots because of its slow ($\mu_r = 31 \pm 6$ mas yr⁻¹, $v_r = 760 \pm 140d_{5.2}$ km s⁻¹) motion. This is most likely a particularly dense cloud in the ambient medium that has been shocked and accelerated first by the SN blast wave and then perhaps accelerated even more by subsequent collision with the SN ejecta. An X-ray- and radio-bright diffuse filament within region SS also moves relatively slowly, with $\mu_r = 56 \pm 5$ mas yr⁻¹ ($v_r = 1380 \pm 120d_{5.2}$ km s⁻¹). This must be a strongly decelerated blast wave that has encountered a much denser ambient medium

than the much faster ($v_r = 4000 \pm 500d_{5.2}$ km s⁻¹) blast wave seen within region FS.

4. SPECTROSCOPY

We fit the data with several models from XSPEC v12.10 (Arnaud 1996), using C-statistics (Cash 1979) and abundances from Grevesse & Sauval (1998). Backgrounds were modeled (not subtracted) as required for use with C-statistics.

4.1. Knots

Spectra of fast-moving ejecta knots are dominated by very strong lines of He-like Ne and Mg ions, as shown in Figure 4 for knot D. These lines are also strong in knots that became visible only in 2018. We modeled the spectrum of the brightest of these new knots (see Figure 4) by an absorbed plane-shock model with pure heavy-element ejecta containing only O, F, Ne, Na, Mg, Al, and Si (with odd- Z element abundances set to solar with respect to O). We obtain a column density $N_H = 1.32(1.22, 1.43) \times 10^{22}$ cm⁻², electron temperature 0.57(0.37, 1.01) keV, ionization age $\tau = 1.03(0.38, 1.87) \times 10^{11}$ cm⁻³ s, and blueshift of 3100(2500, 3800) km s⁻¹ (errors are 90% confidence intervals). Elemental relative abundances with respect to solar are [Ne/O] = 1.17(0.90, 1.54), [Mg/O] = 0.76(0.58, 1.01), and [Si/O] = 0.19(0.11, 0.27), indicating that these ejecta are mostly the products of hydrostatic burning.

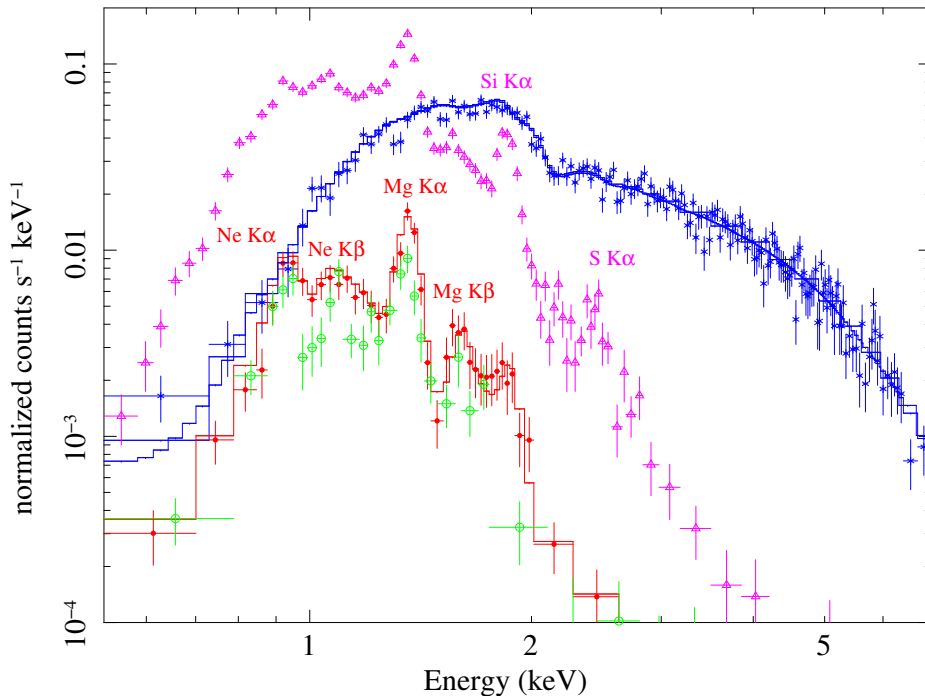


Figure 4. Spectra extracted from the regions shown in Figure 3. Hard nonthermal spectrum of the fast blast wave (blue stars) contrasts sharply with soft thermal spectra of the slowly moving region SS (magenta triangles), the fast-moving knot D (open circles in green), and a bright knot near knot C that was not seen prior to the 2018 observations (filled red circles). Spectral models (see the text for more information) are also shown for the blast wave (blue line) and one of the ejecta knots (red line).

Lines of Ne and Mg are much weaker in the spectrum of the slowly moving region SS than in the ejecta knots (Figure 4). Thermal continuum is clearly visible at higher energies, together with the Si and S $K\alpha$ lines. The Si/Mg $K\alpha$ line ratio is much higher than in the ejecta knots. These are all signatures of normal (cosmic) abundance gas expected in the shocked ambient medium that must be present.

4.2. Blast Wave

We identify the clear edge structure visible in Figure 1 as the blast wave, though projection effects may allow some shocked material to appear farther from the pulsar. The spectrum of the region shown in Figure 3 can be well described either by a power law with column density $N_{\text{H}} = 1.23(1.16, 1.31) \times 10^{22} \text{ cm}^{-2}$ and photon index $\Gamma = 2.33(2.27, 2.40)$, or an srcut model (synchrotron radiation from a power-law electron distribution with exponential cut-off, in which, in the absence of radio data, the mean spectral index was set to -0.5) with $N_{\text{H}} = 1.12(1.05, 1.18) \times 10^{22} \text{ cm}^{-2}$ and rolloff frequency $\nu_{\text{roll}} = 2.54(2.12, 3.28) \times 10^{17} \text{ Hz}$. Either the power-law index or the rolloff frequency values are comparable to those seen in other X-ray-synchrotron-dominated SNR (XSSNR) blast waves (Reynolds 2008). We attribute the lack of thermal emission to the same cause as

in those other XSSNRs: very low ambient density, as is also necessary for the blast wave to have traveled this far in 1710 yr. In this interpretation, the blast wave has not encountered as much material as we infer to be present in the brighter, more eastern regions of RCW 89.

We observe an expansion of the edge at a speed of $(4000 \pm 500)d_{5.2} \text{ km s}^{-1}$. This is certainly adequate to accelerate particles to X-ray emitting energies in less than 1700 yr, and places RCW 89 among fewer than 20 SNRs showing X-ray synchrotron emission from the blast wave. One puzzle is the apparent absence of a radio counterpart to the X-ray edge in 6 cm observations with the Australia Telescope Compact Array (ATCA) that were reported by Leung (2018), but a relatively flat radio-to-X-ray spectral index could cause the radio feature to be difficult to distinguish among the diffuse radio emission that permeates RCW 89.

5. RESULTS AND DISCUSSION

Here we enumerate our results.

1. We find that small structures in RCW 89 are highly dynamic, with large PMs in both radial and transverse directions with respect to the pulsar, and substantial brightness variations, both increasing and decreasing, over the 14 yr covered by the three observations.

2. Expansion velocities for small-scale features range from 5000 km s^{-1} for the fastest knots to less than 1000 km s^{-1} for one feature. However, decelerations are large because the mean expansion velocity for the outer material is about $13,000 \text{ km s}^{-1}$.
3. Most knots have spectra clearly indicative of ejecta, in particular strong lines from Ne and Mg, material synthesized hydrostatically rather than explosively.
4. We have located a feature we identify with the blast wave, expanding at 4000 km s^{-1} , with a lineless spectrum we attribute to synchrotron radiation. This feature has no radio counterpart.

The rapid brightness changes in small knots require high densities. For a knot to appear in 10 yr or less requires an electron density of several hundreds, from our fitted ionization timescales $n_{e,t}$ of order $10^{11} \text{ cm}^{-3} \text{ s}$. While knot velocities are high by absolute standards, the knots have been substantially decelerated in the 1700 yr since the explosion. This deceleration must have occurred fairly recently.

In general, we have a picture of a blast wave from a stripped-envelope SN racing through a low-density wind-blown bubble, and impacting the bubble wall initially in the north. The SN ejecta are mainly diffuse, but some very dense clumps are visible as they impact the wall and shocks are driven into them. The blast wave appears still to be encountering relatively low-density material, and no thermal component of the emission is detectable.

Ejecta with velocities this high have been examined in detail in Cas A, the youngest (350 yr old; Thorstensen et al. 2001) core-collapse SNR in our Galaxy. The densest ejecta in Cas A are optically emitting fast-moving knots (FMKs) that have suffered little deceleration so far. Their estimated preshock densities are uncertain, but they might be as high

as $100\text{--}300 \text{ atoms cm}^{-3}$ (Docenko & Sunyaev 2010). If such knots expand freely for 1710 yr, their preshock densities would drop by a factor of $(1710 \text{ yr}/350 \text{ yr})^3 = 120$. When rapidly shocked and strongly decelerated, they would emit at X-ray (not optical) wavelengths. After compression by a factor of 4 in a strong shock, electron densities would be in the range of $30\text{--}90 \text{ cm}^{-3}$ for the shocked plasma ionization state and abundances we find in the bright new knot whose spectrum is shown in Figure 4. This is only 4–12 times lower than the density inferred by us for this knot. We conclude that the fast-moving ejecta clumps in RCW 89 resemble those seen in Cas A as FMKs in terms of their initial velocities and densities. They might have the same, still not understood origin, presumably related to stripped-envelope SN explosions themselves.

Various proposals have been floated for the relation between the pulsar and PWN and RCW 89. We find little or no evidence for the direct interaction of pulsar-produced phenomena and the X-ray emission of RCW 89. Diffuse emission away from the bright knots has a nonthermal spectrum, but its relatively steep spectral index means it could either be post-shock emission from shock-accelerated electrons, or loss-steepened emission from electrons escaping from the PWN.

The detection of significant X-ray synchrotron emission from the blast wave in RCW 89 makes it the only known SNR showing both a PWN and forward-shock nonthermal X-ray emission.

We acknowledge support by NASA through *Chandra* General Observer Program grant SAO GO7-18068X.

Facilities: CXO

REFERENCES

- Arnaud, K. A. 1996, in ASP Conf. Ser.101, *Astronomical Data Analysis and Systems V*, ed. G. Jacoby & J. Barnes (San Francisco, CA: ASP), 17
- Azzari, L., & Foi, A. 2016, *JSPL*, 23, 1086
- Borkowski, K. J., Reynolds, S. P., Williams, B. J., & Petre, R. 2018, *ApJL*, 868, L21
- Cash, W. 1979, *ApJ*, 228, 939
- Caswell, J. L., Milne, D. K., & Wellington, K. J. 1981, *MNRAS*, 195, 89
- Chevalier, R. A. 2005, *ApJ*, 619, 839
- Docenko, D., & Sunyaev, R. A. 2010, *A&A*, 509, 59
- Gaensler, B. M., Arons, J., Kaspi, V. M., et al. 2002, *ApJ*, 569, 878
- Gaensler, B. M., Brazier, K. T. S., Manchester, R. N., Johnston, S., & Green, A. J. 1999, *MNRAS*, 305, 724
- Grevesse, N., & Sauval, A. J. 1998, *Space Sci. Rev.*, 85, 161
- Kargaltsev, O., Rangelov, B., & Pavlov, G. G. 2013, arXiv:1305.2552
- Krause, O., Birkmann, S. M., Usuda, T., et al. 2008, *Sci.*, 320, 1195
- Leung, W. Y. 2018, PhD thesis, Univ. Hong Kong
- Livingstone, M. A., & Kaspi, V. M. 2011, *ApJ*, 742, 31
- Mills, B. Y., Slee, O. B., & Hill, E. R. 1961, *AuJPh*, 14, 497
- Rest, A., Sinnott, B., Welch, D. L., et al. 2011, *ApJ*, 732, 3
- Reynolds, S. P. 2008, *ARA&A*, 46, 89
- Rodgers, A. W., Campbell, C. T., & Whiteoak, J. B. 1960, *MNRAS*, 121, 103
- Shivvers, I., Modjaz, M., Zheng, W., et al. 2017, *PASP*, 129, 054201
- Thorstensen, J. R., Fesen, R. A., & van den Bergh, S. 2001, *AJ*, 122, 297
- van den Bergh, S., & Kamper, K. W. 1984, *ApJL*, 280, L51
- Yatsu, Y. 2008, PhD thesis, Tokyo Inst. Tech.
- Yatsu, Y., Kawai, N., Kataoka, J., et al. 2005, *ApJ*, 631, 312